THE JOURNAL OF BIOLOGICAL CHEMISTRY VOL. 288, NO. 12, pp. 8691–8701, March 22, 2013

Membrane Microdomains and Cytoskeleton Organization Shape and Regulate the IL-7 Receptor Signalosome in Human CD4 T-cells*[S]

Received for publication, January 2, 2013 Published, JBC Papers in Press, January 17, 2013, DOI 10.1074/jbc.M113.449918

Blanche Tamarit[‡§1], Florence Bugault[‡], Anne-Hélène Pillet[‡§1,2], Vincent Lavergne[‡3], Pascal Bochet[‡¶], Nathalie Garin[‖], Ulf Schwarz, Jacques Thèze[‡], and Thierry Rose[‡4]**

*From the [‡]Institut Pasteur, Département Infection et Epidémiologie, Département d'Immunologie, Unité d'Immunogénétique Cellulaire, 25 Rue du Dr. Roux, 75724 Paris Cedex 15, France, [§]Université Pierre et Marie Curie, Cellule Pasteur-UPMC, 25 Rue du Dr. Roux, 75015 Paris, France, [¶]CNRS UMR3525, 25 Rue du Dr. Roux, 75015 Paris, France, [‖]Leica Microsystems AG, Max Schmidheiny Strasse 201, CH-9435 Heerbrugg, Switzerland, and **Leica Microsystems CMS GmbH, Am Friedrichplatz, D-68165 Mannheim, Germany*

Background: Interleukin-7 is the master regulator of T-cell proliferation.
Results: IL-7 drives its receptor in a membrane microdomain that regulates phosphorylation of associated tyrosine kinases JAK1 and JAK3, anchors IL-7 receptor to cytoskeleton and regulates STAT5 phosphorylation and nuclear translocation.
Conclusion: Membrane microdomains and cytoskeleton scaffold IL-7R-signalosomes and assist signaling protein transport.
Significance: Transient membrane and cytoskeleton organization shapes IL-7-signaling mechanisms in CD4 T-cells.

Interleukin (IL)-7 is the main homeostatic regulator of CD4 T-lymphocytes (helper) at both central and peripheral levels. Upon activation by IL-7, several signaling pathways, mainly JAK/STAT, PI3K/Akt and MAPK, induce the expression of genes involved in T-cell differentiation, activation, and proliferation. We have analyzed the early events of CD4 T-cell activation by IL-7. We have shown that IL-7 in the first few min induces the formation of cholesterol-enriched membrane microdomains that compartmentalize its activated receptor and initiate its anchoring to the cytoskeleton, supporting the formation of the signaling complex, the signalosome, on the IL-7 receptor cytoplasmic domains. Here we describe by stimulated emission depletion microscopy the key roles played by membrane microdomains and cytoskeleton transient organization in the IL-7-regulated JAK/STAT signaling pathway. We image phospho-STAT5 and cytoskeleton components along IL-7 activation kinetics using appropriate inhibitors. We show that lipid raft inhibitors delay and reduce IL-7-induced JAK1 and JAK3 phosphorylation. Drug-induced disassembly of the cytoskeleton inhibits phospho-STAT5 formation, transport, and translocation into the nucleus that controls the transcription of genes involved in T-cell activation and proliferation. We fit together the results of these quantitative analyses and propose the following mechanism. Activated IL-7 receptors embedded in membrane microdomains induce actin-microfilament meshwork formation, anchoring microtubules that grow radially from rafted receptors to the nuclear membrane. STAT5 phosphorylated by signalosomes are loaded on kinesins and glide along the microtubules across the cytoplasm to reach the nucleus 2 min after IL-7 stimulation. Radial microtubules disappear 15 min later, while transversal microtubules, independent of phospho-STAT5 transport, begin to bud from the microtubule organization center.

IL-7 is a crucial cytokine in the immune system (1, 2) in that it induces the production of CD4 T-lymphocytes from precursor cells in the thymus, regulates their proliferation, and contributes to the homeostasis of mature CD4 T-cells in peripheral blood. IL-7 is secreted by stromal cells in red marrow, thymus, keratinocytes, dendritic cells, and endothelial cells (3). It binds to a heterodimeric receptor, IL-7R, made up of two glycosylated subunits: IL-7Rα (CD127, 65 kDa) (4), specific to IL-7 and thymic stromal lymphopoietin (5), and the common γ chain (γc, CD132, 56 kDa) shared by IL-2, 4, 7, 9, 15 and 21 receptors (2). These two chains have common ancestors and share the same topology; both chains are embedded in the membrane by a single-pass transmembrane helix that connects the immunoglobin fold structured ectodomain to the unstructured cytoplasmic domain (6).

IL-7Rα is expressed at the surface of quiescent cells and gradually disappears within 12 h of activation by IL-7 (7–9). Conversely, γc is weakly expressed at the surface of quiescent CD4 T-cells, but activation by IL-7 rapidly up-regulates its expression, which peaks after 12 h and lasts for as long as 48 h. The heterodimer is formed prior to IL-7 binding (10). IL-7 has high affinity for the IL-7R heterodimer ($K_d \sim 35 \cdot 10^{-12}$ M) and shifts the equilibrium of receptor assembly. By contrast, IL-7 has low affinity for its single proprietary chain, IL-7Rα ($K_d \sim 3 \cdot 10^{-9}$ M) and poor affinity for γc ($K_d > 250 \cdot 10^{-9}$ M) (11). The cytoplasmic domain of IL-7Rα is long (195 residues), whereas that of γc is shorter (86 residues). Both domains are responsible for binding

* This work was supported in part by Institut Pasteur and its Transversal Research Program (PTR 424).
[S] This article contains supplemental Experimental Procedures and Figs. S1–S4.
[1] Supported by fellowships from the Ministère de l'Education Nationale et de la Recherche.
[2] Present address: Institut Curie, 26 rue d'Ulm, 75248 Paris cedex 5, France.
[3] Present address: University of Queensland, Brisbane St. Lucia QLD4072, Australia.
[4] To whom correspondence should be addressed. Tel.: 33-145-68-85-99; Fax: 33-145-68-82-28; E-mail: rose@pasteur.fr.

a large array of proteins involved in signaling pathways that support cell survival and proliferation (2). These proteins include Janus kinases, JAK1 and JAK3 (bound by IL-7Rα and γc, respectively), that are involved in the JAK/STAT pathway. JAK1 and JAK3 recover their Tyr kinase activity when tethered in close contact by the IL-7-activated receptor. They phosphorylate themselves and then the IL-7Rα carboxyl-terminal Tyr (Tyr(P)-456). This Tyr(P)-456 provides a single binding site for STAT1, STAT3, and mainly STAT5a and STAT5b. Bound STATs are then phosphorylated by the activated pJAK1·pJAK3[5] complex (12). After phosphorylation, the STATs dissociate, dimerize, and are translocated into the nucleus, where they induce transcription of gene clusters involved in cell programs (12). MAPKs and PI3K/Akt (signaling serine/threonine kinase) pathways are also triggered by IL-7·IL-7R binding and give rise to mitogenic and anti-apoptotic signals (1, 2). Although a wealth of information is available on the various kinases involved in IL-7 signal transduction, less is known about the formation of the signaling complex and its molecular mechanism.

We have previously shown that IL-7 binds to its preassociated receptor and then induces migration of the complex into membrane microdomains, as observed by flotation ultracentrifugation through a sucrose gradient and by diffusion measurements in living cells using fluorescence autocorrelated spectroscopy (FCS) (10). These embedded complexes are then confined by the cytoskeleton, as suggested by slowed receptor diffusion measured by FCS, and are released by cytoskeleton disassembly drugs (10). We used mass spectrometry (MS) to analyze the content of the protein complex immunoprecipated with IL-7Rα after IL-7-activation and CD4 T-cell lysis in Triton X-100 buffer (10). We found that activated IL-7R is associated with many proteins known to be present in cytoskeleton and membrane microdomains and with proteins involved in several signaling pathways (10).

In the study reported here, we used superresolution optical microscopy by stimulated emission depletion (13–15) to observe structures smaller than the theoretical diffraction limit. We showed for the first time how IL-7 in human primary CD4 T-lymphocytes induces the rapid formation of 1) membrane microdomains, 2) dual actin-cortex organization, and 3) transient radial microtubules that bridge plasma and nuclear membranes. We demonstrated that IL-7·IL-7R compartmentalization in membrane microdomains regulates JAK phosphorylation and that confinement by the cytoskeleton upon IL-7 binding controls STAT phosphorylation, transport, and translocation into the nucleus. We also herein provide a step-by-step description of the IL-7-induced JAK/STAT signaling pathway that is central to CD4 T-cell activation and proliferation.

MATERIALS AND METHODS

Purification of Human CD4 T-lymphocytes—Venous blood was obtained from healthy volunteers through the Etablissement Français du Sang (Centre Necker-Cabanel, Paris). CD4 T-cells were purified from peripheral blood mononuclear cells, checked for homogeneity and activation state, and cultured in microplates, as described previously (10) and detailed in the supplemental material. Cells were activated with 2 nM recombinant glycosylated human IL-7 (Cytheris) at 37 °C in a temperature-controlled water bath and a 5% CO_2 humidified atmosphere.

Confocal and STED Microscopy—Images were acquired above the diffraction limit on an inverted laser-scanning confocal microscope (LSM700, Zeiss) as detailed in the supplemental material. Images were acquired below the diffraction limit on two DM16000CS/SP5 inverted laser-scanning confocal microscopes using either continuous wave excitation STED (CW-STED; Leica) (14) or pulsed excitation STED (STED; Leica) (13).

Cell preparation and labeling of specific proteins is described in detail in the supplemental material. Briefly, cells were purified, equilibrated in RPMI for 2 h at 37 °C, and then loaded on polylysine-coated coverglasses for 20 min at 37 °C. When needed, immobilized cells were treated with either cytochalasin D (CytD; Sigma), colchicin (Col; Sigma), or cholesterol oxidase (COase; Sigma) for 30 min or sphingomyelinase (SMase; Sigma) for 5 min at 37 °C and then activated with 2 nM IL-7. Cells were fixed from 1 to 60 min after the addition of IL-7 with 1.5% paraformaldehyde (PFA; Sigma) for 15 min at 37 °C and then permeabilized when necessary for 20 min in ice-cold 90% methanol/water solution when required for cytoplasmic labeling. Cells were then rehydrated for 15 min in PBS plus 5% fetal bovine serum (FBS) and then labeled. For pSTAT5 kinetics, cells were pretreated with acidic buffer and washed twice in PBS/FBS before fixation (10). GM1 gangliosides were labeled with AlexaFluor-coupled cholera toxin subunit B (CtxB-AlexaFluor488 or CtxB-AlexaFluor647; Invitrogen) on non-permeabilized cells that were either fixed with PFA or not. The other proteins were targeted with corresponding primary antibodies. The secondary antibodies used for pulsed STED microscopy consisted of anti-mouse IgG-Chromeo494, anti-rabbit IgG-Chromeo494, and anti-rabbit IgG-Atto647 (Active Motif). Anti-mouse IgG-AlexaFluor488 (Invitrogen) and anti-rabbit IgG-AlexaFluor488 (Invitrogen) were used for CW-STED and confocal microscopy. Anti-mouse IgG-AlexaFluor633 was used for confocal microscopy. Cells were mounted in Vectashield/DAPI medium (Vector Laboratories) for confocal microscopy and in Mowiol (4-88; Sigma) supplemented with antifading Dabco (35 mg/ml; Sigma) for STED microscopy.

Receptor Chain Diffusion Rate Analysis by Fluorescence Cross-correlated Spectroscopy—All protein diffusions at the surface of living human CD4 T-cells were acquired and analyzed in the absence and presence of raft and cytoskeleton inhibitors by spot variation FCS (16) using an inverted laser-scanning confocal microscope (LSM510, Zeiss), combined with a ConfoCor2 FCS system (Zeiss), as described previously (10), and detailed in the supplemental material.

Protein Assays by Flow Cytometry—Procedures are detailed in the supplemental material. Briefly, CD4 T-cells were treated with drugs, activated with IL-7, and then fixed with PFA. GM1 was assayed at the surface of non-permeabilized cells using

[5] The abbreviations used are: pJAK, phosphorylated JAK; pSTAT, phosphorylated STAT; FCS, fluorescence autocorrelated spectroscopy; GM1, monosialotetrahexosyl ganglioside; MTOC, microtubule organization center; STED, stimulated emission depletion; CW-STED, continuous wave excitation STED; CytD, cytochalasin D; Col, colchicin; COase, cholesterol oxidase; sphingomyelinase; PFA, paraformaldehyde; CtxB, cholera toxin subunit B.

CtxB-AF488. pSTAT5 was assayed in permeabilized cells using ice-cold 90% methanol/water, as described previously (10). The kinetics of IL-7-induced actin and tubulin polymerization were determined by cytometry. Activation in 96-well plates was stopped by centrifugation (350 × *g*) for 1 min at 4 °C. CD4 T-cells were labeled at the cell surface (anti-CD4-ECD) in 1% FBS for 30 min at 4 °C. Cells were washed in cold PBS, centrifuged, and then permeabilized by 0.5% Triton X-100 for 10 min on ice. PFA was added (1.5% final), and the cells were centrifuged for 5 min. They were then washed in cold PBS and incubated for 30 min in PBS containing 5% FBS at 4 °C with anti-actin-AF647 (sc1616, Santa Cruz Biotechnology, Inc.) and anti-tubulin-AF488 (sc5286, Santa Cruz Biotechnology, Inc.). Cells were washed in cold PBS and analyzed on a Cyan LX™ cytometer (DakoCytomation) using FlowJo version 8.3.3 data analysis software (Tree Star).

Western Blot Analysis—Immunoprecipitations were performed from centrifuged lysates after treatment of purified CD4 T-cells with Triton X-100 buffer using the indicated primary antibodies and immobilized protein G on Sepharose-4G (GE Healthcare), and immunoprecipitated protein samples were analyzed by Western blotting as described in the supplemental material.

RESULTS

STED Microscopy Analysis of IL-7-induced Membrane Microdomains at the Surface of Human CD4 T-lymphocytes—Human CD4 T-cells were isolated from the blood of several healthy donors. Cells were re-equilibrated in culture medium at 37 °C and 5% CO_2 for 2 h and then activated by 2 nM IL-7 for 10 min. Membrane microdomains were labeled through ganglioside (GM1) with cholera toxin B (CtxB) tagged with AlexaFluor488. *Z*-stacks of images were acquired by superresolution optical microscopy processing CW-STED. Flattened three-dimensional reconstructions of the half-cell tops are shown in Fig. 1, *a*–*c*, and corresponding images at full resolution are shown in supplemental Fig. S1. IL-7-activated CD4 T-lymphocytes showed several hundred dense, circular spots. These spots were sparsely scattered over the surface of quiescent cells. The number and size of these GM1-enriched membrane microdomains were averaged over 100 CD4 T-cells (Fig. 1, *d* and *e*): 307 ± 50 spots/cell of 90-nm diameter in IL-7-activated cells, 12 ± 6 spots/cell of 170-nm diameter in quiescent cells. IL-7-induced spots were observed over the entire surface of the cells. Spot distribution density was sometimes asymmetrical, but no clustering was observed. The formation of these microdomains started about 1 min after adding IL-7. Half the spots were formed after 5 min, and the maximum was reached after 15 min (Fig. 1*f*). The number of spots then slowly decreased, whereas spot diameter increased (Fig. 1*g*). No such spots were observed on IL-7-activated CD4 T-cells after 30 min of treatment with COase and 5 min of treatment with SMase, as shown in Fig. 1*c*. These spots, or membrane microdomains, are large lipid rafts, enriched in cholesterol, sphingomyelin, and GM1. GM1 distribution changed upon IL-7 activation, but the overall number of GM1 at the surface of T-cells was only slightly affected over the first 15 min

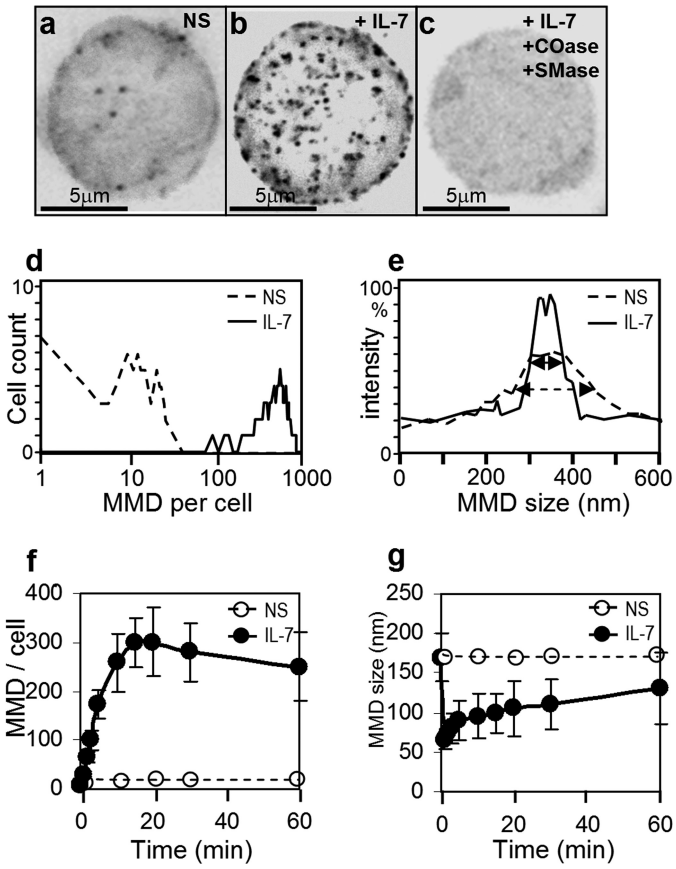

FIGURE 1. **Membrane microdomain formation induced by IL-7 at the CD4$^+$ T-cell surface, resolved by STED microscopy.** The binding of CtxB-AF488 on the GM1-enriched region was imaged by CW-STED microscopy after 5 min of activation by IL-7 (*b*) at the surface of nonstimulated (*NS*) lymphocytes (*a*) or COase- and SMase-treated cells (*c*). Sliced images of the half-cell top at the opposite side of the coverglass were flattened. Image colors were inverted and converted to *grayscale*. Original images are shown in supplemental Fig. S1. Total GM1 binding per cell was assayed by cytometry and plotted in supplemental Fig. S2. The number of GM1-enriched membrane microdomains was averaged from 100 CD4$^+$ T-cells (*d*) from slides shown in *a* and *b*. The size of membrane microdomains was averaged from 100 cells from the same slides; the measurement of CtxB-AF488 fluorescence intensity in one membrane microdomain is shown for nonstimulated (*dashed line*) and IL-7-stimulated cells (*continuous line*) (*e*). Membrane microdomain number (*f*) and size (*g*) are plotted *versus* time after IL-7 activation. *Error bars*, S.E.

of activation, as shown by flow cytometry analysis of GM1 labeled with CtxB-AF488 (supplemental Fig. S2).

Membrane Domain Disassembly Inhibits JAK Phosphorylation—In order to investigate the role played by membrane compartmentalization in the IL-7-induced phosphorylation of JAKs and STATs, we analyzed the kinetics of IL-7-induced JAK1, JAK3, and STAT5 phosphorylation before and after treatment with optimal concentrations of lipid raft inhibitors (COase and SMase). Cytoplasmic concentrations of pJAK1 (Tyr(P)-1034/Tyr(P)-1035), pJAK3 (Tyr(P)-980/Tyr(P)-981), and pSTAT5 (Tyr(P)-694) were compared by averaging densitometric analyses of ECL bands from five Western blots (Fig. 2). In the absence of any inhibitors, pJAK1 and pJAK3 started to accumulate 1 min after IL-7 activation, reached 50% of the maximum concentration after 5 min, peaked after 15 min, and decreased thereafter (Fig. 2, *a*, *c*, and *d*). In the presence of COase and SMase, JAK1 and JAK3 were phosphorylated 10 times more slowly after the addition of IL-7, peaked 60 min later at only 25% of the optimal concentration observed in the absence of raft inhibitors, and then decreased after-

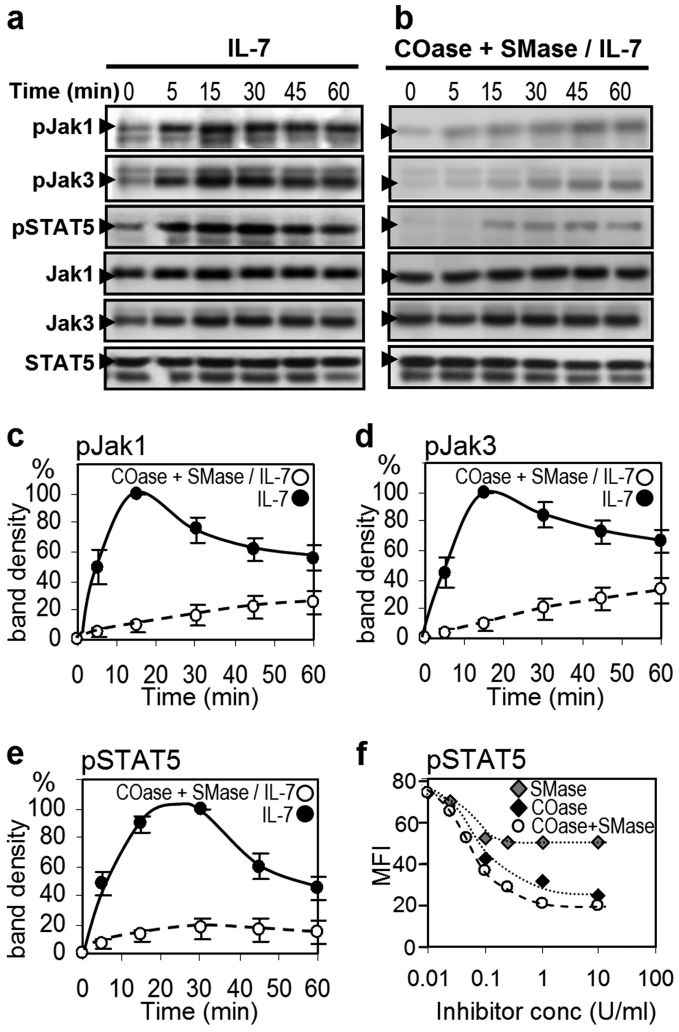

FIGURE 2. **Disassembly of membrane microdomains inhibits JAK1 and JAK3 phosphorylation kinetics.** JAK1, JAK3, and STAT5 phosphorylation was measured by Western blotting during IL-7 activation of CD4 T-cells in the absence (*a*) or in the presence (*b*) of raft inhibitors (1 unit/ml, i.e., 31 μM COase and 0.1 unit/ml, i.e., 2.7 μM SMase). The kinetics of pJAK1 (*c*), pJAK3 (*d*), and pSTAT5 (*e*) accumulation in the presence or absence of combined lipid raft inhibitors were plotted from band density (sum of pixel intensities in a *rectangle boxing* the band divided by the corresponding band of the unphosphorylated species and corrected for the offset at time 0). Maximum density was set to 100%, and minimum density was set to 0 for a treated/untreated blot pair. Percentage values were averaged from five blot pairs (five independent CD4 T-cell donors). *Error bars*, S.E. The results of intracellular pSTAT5 assays by FACS were plotted against inhibitor concentration 15 min after IL-7 activation, without and with lipid raft inhibitors, separately (COase, SMase) or in unit/unit combination (COase + SMase) (*f*).

ward (Fig. 2, *b*, *c*, and *d*). Lipid raft inhibitors affected both JAK phosphorylation efficiency and kinetics. In untreated cells, pSTAT5 reached 50% of the plateau concentration in the cytoplasm 7 min after activation and reached the plateau concentration after 15 min (Fig. 2, *a* and *e*). In the presence of raft inhibitors, only 17% of the pSTAT5 plateau was reached (Fig. 2, *b* and *e*). A quantitative analysis of overall intracellular pSTAT5 concentrations by flow cytometry corroborated the effects of the combined inhibitors and their kinetics and showed that COase has a greater inhibitory effect than SMase (Fig. 2*f*).

IL-7 Induces Transient Cytoskeleton Structuring—Investigations by pulsed STED microscopy showed that IL-7 induces a two-step structural organization of cytoskeleton in CD4 T-cells (Fig. 3). Early structuring occurred 1 min after IL-7 was added. We noted, in quiescent cells, that actin was mainly concentrated in the vicinity of the plasma membrane and was diffuse elsewhere in the cytoplasm (Fig. 3, *a* and *d*). Tubulin was diffused throughout the cytoplasm (Fig. 3, *a* and *f*). After IL-7 activation, actin formed two dense layers: the first beneath the plasma membrane and the second surrounding the nuclear membrane (Fig. 3, *b* and *e*). Strikingly, tubulin was seen to form rods organized radially through the cytoplasm (250–1000 nm in length) and bridging plasma and nuclear membranes (Fig. 3, *b* and *g*). These rods showed labeling patterns consistent with microtubules, the two ends of which were deeply anchored in both actin cortexes. Actin layers appear denser at the junction point with tubulin rod patterns. We counted 5–25 tubulin rod patterns per 500-nm thickness of cell slice image (23 threads in Fig. 3*b*, six of which are shown in the *enlarged boxed area* in Fig. 3*g*). No such threads were observed in non-activated control cells (Fig. 3*f*). These radial microtubules disappeared 15 min after the addition of IL-7 and had an individual life span of about 5–10 min. In the largest space in the cytoplasm, nascent microtubules budded from the microtubule organization center (MTOC) 10 min after the addition of IL-7. Whereas the radial microtubules disappeared, transversal microtubules grew from the MTOC in a star pattern (Fig. 3*c*) to surround the nucleus after 45 min, as detailed by pulsed STED microscopy in Fig. 3*h* and supplemental Fig. S3 (full resolution). Fig. 3*h* shows nine microtubule bundles radiating from the MTOC and the separation of each into single fibers. The *boxed region* in Fig. 3*h* is *enlarged* in Fig. 3*j*, which shows microtubule details. These long transversal microtubules in Fig. 3*j* were comparable in section diameter and staining irregularity with the short radial microtubules shown in Fig. 3*g*. These structures were very fuzzy in conventional microscopy (Fig. 3, *i* and *k*). Logically, IL-7 failed to induce any cytoskeleton structural organization 30 min after the cells had been treated with drugs that inhibit microfilament assembly (CytD) or microtubule assembly (Col) and showed fuzzy actin and tubulin distribution as seen in non-stimulated cells.

The kinetics of IL-7-induced actin and tubulin polymerization were determined by cytometry. Cells were permeabilized with Triton X-100 and then fixed with PFA. Actin and tubulin were labeled with anti-actin-AF647 and anti-tubulin-AF488 (Fig. 3*l*). IL-7 increased the levels of actin and tubulin detected in the first 10 min; actin polymerization in microfilaments and tubulin assembly in microtubules were seen to stabilize these structures in the Triton-permeabilized cells. The decrease in tubulin after 15 min may be interpreted as due to disassembly of the IL-7-induced radial microtubules preceding the formation of transversal microtubules from the MTOC. Investigations after treatment with CytD and then IL-7 activation (5 min) confirmed that microtubule formation is dependent on microfilament organization (Fig. 3*m*). Observations by STED microscopy of cells treated with Col confirmed that microfilament organization beneath the plasma membrane is independent of microtubule formation, but the perinuclear actin cortex depends on the presence of microtubules.

Actin Cortex Anchors Activated IL-7 Receptors—We have previously measured by FCS the diffusion rate D_{eff} of IL-7Rα (0.21 $\mu m^2/s$) and shown by fluorescence cross-correlated spec-

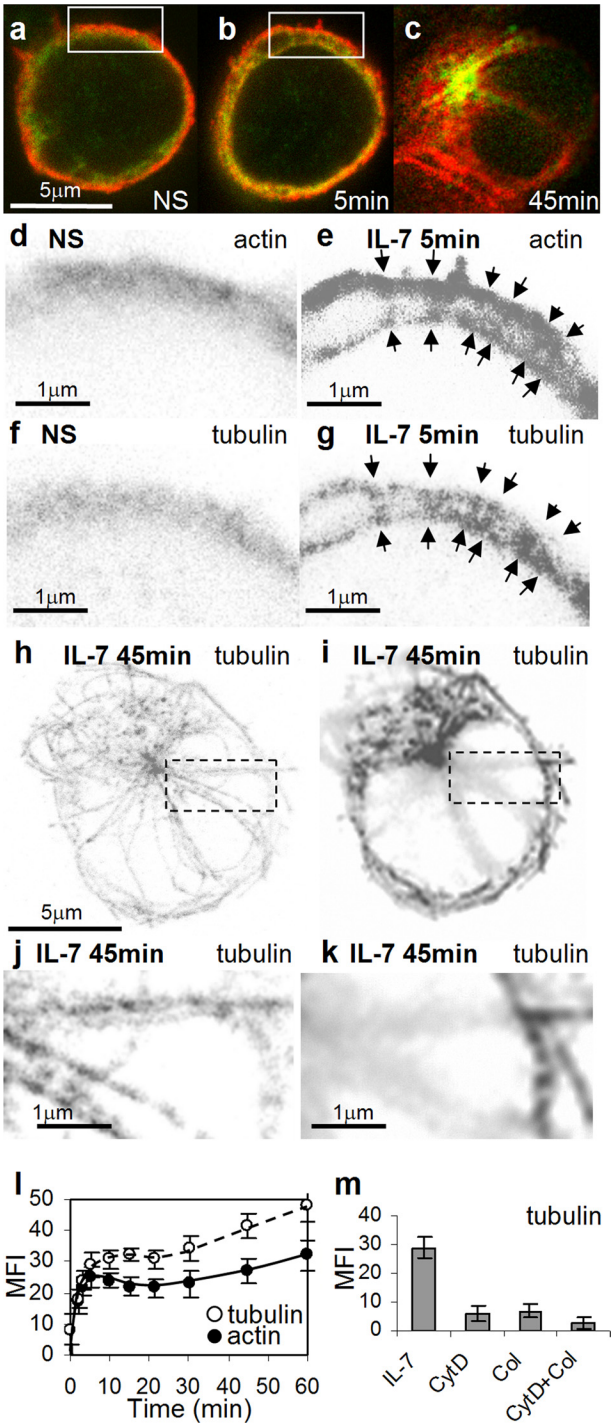

FIGURE 3. **IL-7 induces cytoskeleton structuring observed by STED microscopy.** Microfilament and microtubule organization was compared by pulsed-STED microscopy before (*a*), 5 min (*b*), and 45 min (*c*) after IL-7 activation of human primary CD4 T-cells. Tubulin from microtubules was labeled with mouse anti-tubulin and anti-mouse-chromeo494 (*green*), and actin from microfilaments was labeled with rabbit anti-actin and anti-rabbit Atto647 (*red*). Details of actin organization are shown in *d* and *e*, and details of tubulin organization are shown in *f* and *g* from the *boxed area* in nonstimulated and IL-7-activated cell images (*a* and *b*, respectively). *Image colors* were inverted and converted into *grayscale*. Original full resolution images are shown in supplemental Fig. S3). Radial microtubules passing through the cytoplasm 5 min after IL-7 activation are indicated by *arrows* and contrast with the cytoplasm of unactivated cells. Images show tubulin organization in cells 45 min after activation, by STED (*h*) and regular confocal microscopy (*i*) with the *boxed area enlarged* in corresponding *panels* (*j* and *k*). Kinetics of IL-7-induced actin and tubulin polymerization, by cytometry, are plotted in *l* with mean fluorescence intensity (*MFI*) *versus* time (min) with *bars* indicating S.E. from five independent experiments (five donors). Cells were permeabilized by 0.5% Triton X-100 and then fixed by 1.5% PFA. Actin and tubulin were labeled with anti-actin-AF647 and anti-tubulin-AF488. Mean fluorescence intensity assays by cytometry were then performed with the same labeling after Col and CytD treatments (30 min) and then IL-7 activation for 5 min (*m*).

troscopy that the addition of IL-7 slows the diffusion of its preassembled receptor IL-7Rα·γc from 0.17 down to 0.02 $\mu m^2/s$ (10). We have also demonstrated that receptor slowing is a consequence of its IL-7-induced recruitment by the cytoskeleton. We detail here the respective roles of microfilaments and microtubules. The diffusion rate and confinement time of the labeled complex were measured by spot variation FCS (16, 17) in live CD4 T-cells. Diffusion rate is inversely proportional to the slope of the diffusion time *versus* spot area (ω_0^2) plot. Confinement time τ_0 was extrapolated in the same plot as the *y* intercept. Diffusion plots of the IL-7Rα·mAb-AF488·IL-7biotin·SAF633 complex are given herein (Fig. 4*a*), along with bar graphs comparing diffusion rates and confinement times (Fig. 4*b*) for increasing doses of CytD. Details of these measurements are given in supplemental Fig. S4. The dose-response obtained with CytD illustrates receptor release for diffusion when actin filaments are depolymerized. The diffusion rate of activated receptors was maximal from 20 μM CytD (D_{eff} = 0.23 $\mu m^2/s$) (Fig. 4*b*). Microtubule depolymerization by Col did not release any activated receptors, and Col did not increase the effect of CytD on receptor diffusion (Fig. 4*b*). Lipid raft inhibitors (COase, SMase, or COase + SMase) failed to release receptors confined in actin-scaffold structures (Fig. 4*b*), but in the presence of CytD, treatment with COase + SMase did increase the diffusion rate of cytokine-bound receptors (D_{eff} = 0.35 $\mu m^2/s$); they diffused even more rapidly than cytokine-free receptor (D_{eff} = 0.17 $\mu m^2/s$) and IL-7Rα single chain (D_{eff} = 0.21 $\mu m^2/s$) on untreated cells, and confinement time was zero (*i.e.* characteristic of free two-dimensional diffusion out of membrane microdomains). The activated receptors diffused freely as the cytoskeleton meshing the membrane inlet vicinity was disassembled. We noted that although actin microfilaments anchored IL-7-activated receptors even in the absence of microtubules and membrane microdomains, the anchoring kinetics under these conditions were altered.

Cytoskeleton Disassembly Inhibits STAT Phosphorylation—The involvement of IL-7-induced cytoskeleton organization in the JAK/STAT pathway was assessed by comparing the effect of cytoskeleton inhibitors on the IL-7-induced phosphorylation of JAK1, JAK3, and STAT5 (Fig. 5). We determined the kinetics of pJAK1 (Tyr(P)-1034/Tyr(P)-1035), pJAK3 (Tyr(P)-980/Tyr(P)-981), and pSTAT5 (Tyr(P)-694) accumulation in the cytoplasm by Western blotting after treatment with CytD (20 μM) and Col (10 μM) (Fig. 5*b*) and compared the results with pJAK and pSTAT5 concentrations in the absence of these cytoskeleton inhibitors (Fig. 5*a*). Band densities were averaged from five Western blot pairs processed from the cells of five healthy blood donors. Cytoskeleton assembly inhibitors had only weak effects on the kinetics of JAK1 and JAK3 phosphorylation (Fig. 5, *c* and *d*). Conversely, STAT5 phosphorylation was substantially delayed and reduced (Fig. 5*e*). When T-cells were pretreated with CytD and Col, STAT5 phosphorylation was eight times slower and peaked 45 min after the addition of

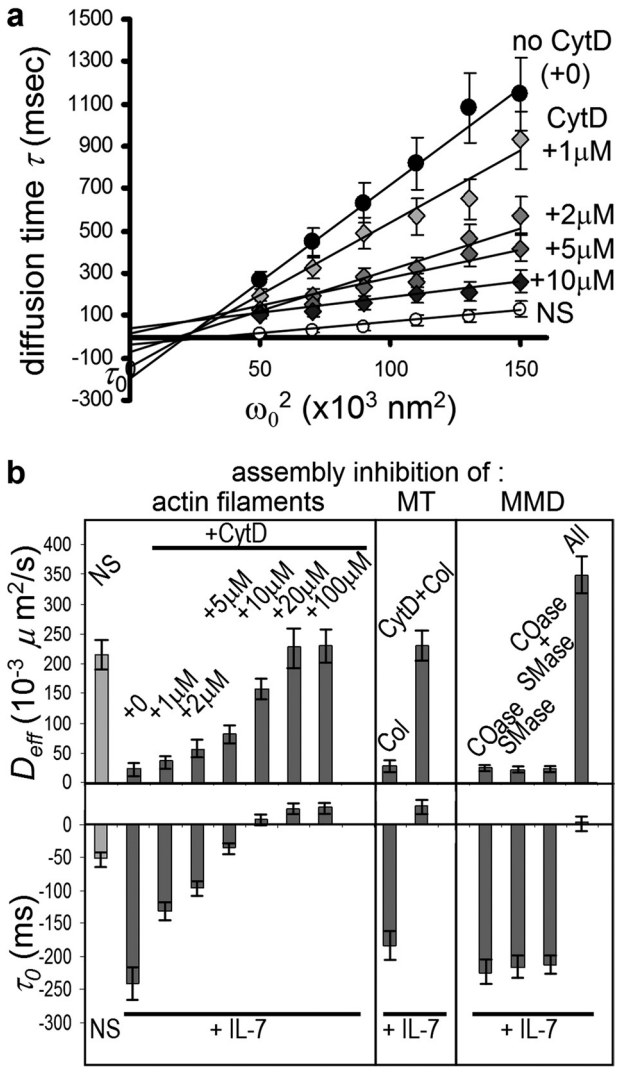

FIGURE 4. **Actin microfilament meshwork anchors activated IL-7 receptors, and receptor embedding in membrane microdomains is independent of this anchoring.** Two-dimensional diffusion of IL-7Rα labeled by AF488-coupled monoclonal antibody anti-IL-7Rα was measured at the surface of living CD4 T-cells by FCS and fluorescence cross-correlated spectroscopy. Diffusion times τ_D (in 10^{-3} s) in the presence of IL-7biotin·SAF633 are plotted *versus* the surface area ω^2 intercepted by the confocal volume (in 10^3 nm^2): autocorrelation function *(ACF)* of IL-7Rα·mAb-AF488 in the absence of IL-7 (○; *NS*) and crosscorrelation function *(CCF)* of IL-7Rα·mAb-AF488 with IL-7biotin·SA633 without CytD (●) in the presence of increasing concentrations of CytD (◆). Diffusion plots (fluorescent particle diffusion time *versus* surface area intercepted by the variable confocal volume) are shown in *a*. All cross-correlation curves are detailed in supplemental Fig. S4. Slopes of the linear regression give effective diffusion rates D_{eff}, and *y* intercepts extrapolate confinement time τ_0, as described previously (16, 17). *b*, D_{eff} (*top*) and τ_0 (*bottom*) are shown in the *bar graph* for IL-7R·Ab-AF488 in the absence of IL-7 (*NS*), in the presence of IL-7biotin·SA633 without inhibitor (+0), and then with different pretreatments using the following inhibitors: CytD (from 1 to 100 μM), Col (10 μM), CytD (20 μM) + Col (10 μM), COase (1 unit/ml, i.e., 31 μM), SMase (0.1 unit/ml, i.e., 2.7 μM), and COase + SMase. *All*, COase + SMase + CytD + Col. *Error bars*, S.E. from five independent experiments.

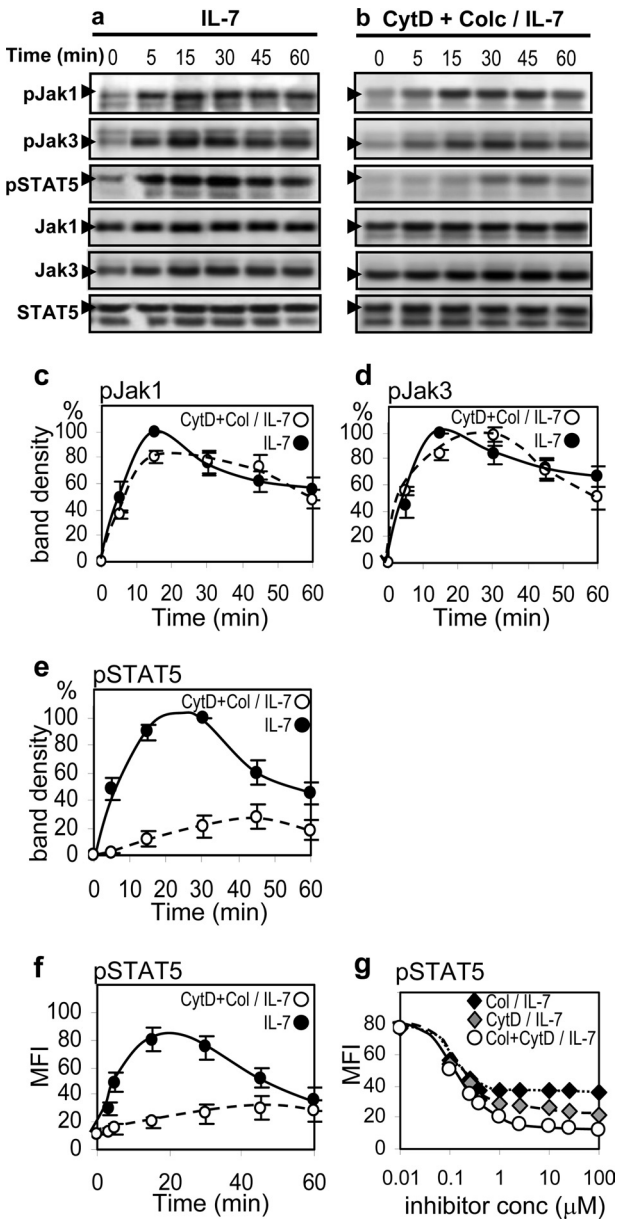

FIGURE 5. **Cytoskeleton disassembly inhibits STAT5 phosphorylation.** JAK1 and STAT5 phosphorylation kinetics were analyzed by Western blotting during IL-7 activation of CD4 T-cells in the absence (*a*) or in the presence of cytoskeleton inhibitors (20 μM CytD and 10 μM Col) (*b*). Maximum density was set to 100% and minimum to 0 for a treated/untreated blot pair. Percentage values were averaged from five blot pairs (five independent CD4 T-cell donors) (*c* and *d*). *Bars*, S.E. Band densities were computed from the sum of pixel intensities in a *rectangle boxing* the *band* divided by the corresponding band of the unphosphorylated species and corrected for the offset at time 0. Mean fluorescence intensity (*MFI*) of intracellular pSTAT5 staining measured by FACS were also averaged from five independent CD4 T-cell donors and was plotted *versus* time (*e*). The dose-dependent inhibition of the phosphorylation response to IL-7 activation was measured by FACS (*f*).

IL-7 at only 28% of the optimal pSTAT5 concentration observed in the absence of drugs and then decreased afterward (Fig. 5*e*). These observations were confirmed in intracellular pSTAT5 assays by flow cytometry summing cytoplasmic and nuclear concentrations (Fig. 5*f*). Col, CytD, and Col + CytD were seen to cause a dose-dependent alteration in pSTAT5 concentrations measured by flow cytometry, which fell to a minimum from Col >1 μM and showed a slow slope drift with CytD >2 μM (Fig. 5*g*). CytD had a more marked effect than Col on pSTAT5 plateau concentrations. Col accentuated the inhibitory effect of CytD when used in combination.

Cytoskeleton Disassembly Alters STAT Transport Kinetics and Translocation—Because IL-7 was observed to induce rapid and marked cytoskeleton reorganization, we investigated the effects of CytD and Col on pSTAT5 transport across the cyto-

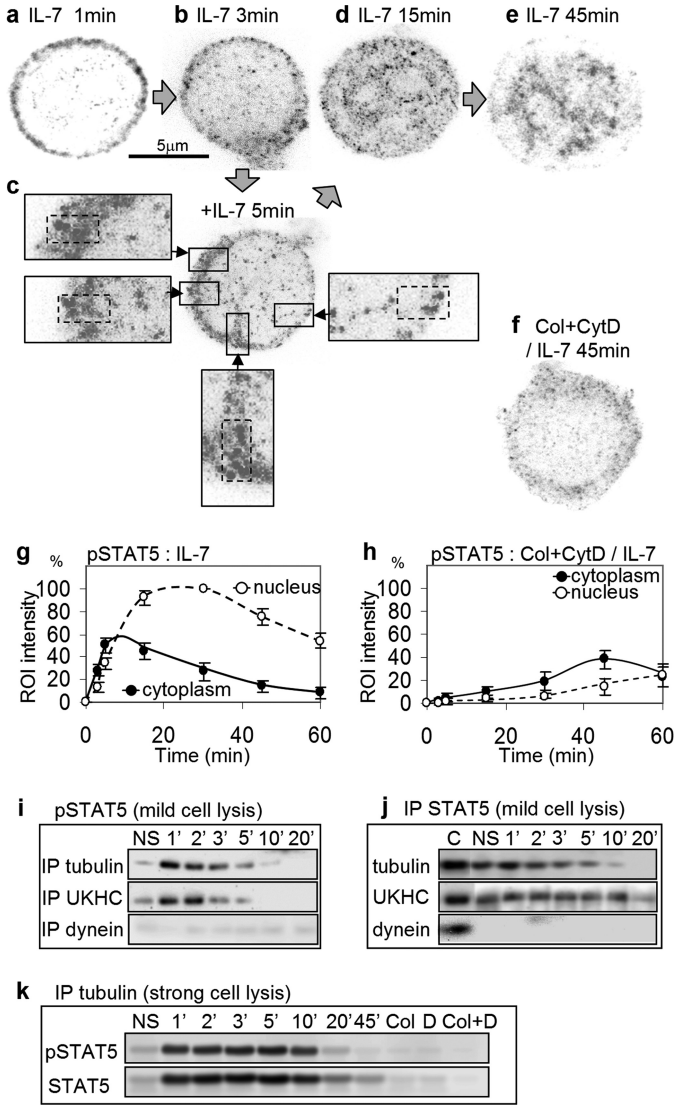

FIGURE 6. **Kinetics of kinesin-assisted pSTAT5 transport and translocation into the nucleus observed by STED microscopy after IL-7 activation.** pSTAT5 was labeled with a specific primary mAb and then a secondary anti-rabbit antibody, Atto647, on PFA-fixed cells 1, 3, 5, 15, and 45 min after the addition of IL-7 and imaged on a pulsed STED microscope (*a–e*). Details of pSTAT threads are *boxed* from the 5 min image (*c*). *f*, image obtained 45 min after the addition of IL-7 in a cell pretreated with CytD + Col. Pixel intensity sum for the nucleus and cytoplasm areas (*ROI*, region of interest) was averaged for five cells and plotted against IL-7 activation time in the absence (*g*) or in the presence of cytoskeleton inhibitors (*h*). pSTAT5 (90 kDa) was analyzed by Western blotting after immunoprecipitation with anti-tubulin, anti-UKHC, and anti-dynein from 1 to 20 min after IL-7 activation (*i*). Tubulin (54 kDa), UKHC (120 kDa), and dynein (75 kDa) immunoprecipitations (*IP*) with anti-STAT5 were analyzed against activation time (*j*); *lane C* shows the unprecipitated lysate control. pSTAT5 and STAT5 are labeled from proteins immunoprecipitated by anti-tubulin from cells thoroughly lysed by 1% Triton X-100 buffer and then frozen and thawed twice and assayed from 1 to 45 min in the absence or presence of cytoskeleton inhibitors separately (CytD and Col) or in unit/unit combination (CytD + Col) (*k*). *Error bars*, S.E.

plasm and translocation into the nucleus because this signaling intermediate is phosphorylated below the plasma membrane and is known to promote the transcription of many nuclear genes in synergy with other factors. We used pulsed STED microscopy to compare pSTAT5 distribution kinetics in IL-7-induced CD4 T-cells in the absence or in the presence of cytoskeleton inhibitors before activation (Fig. 6). In the absence of inhibitors, pSTAT5 appeared in the cytoplasm, below the plasma membrane, 1 min after the addition of IL-7 (Fig. 6*a*), peaked from 5 to 10 min, decreased afterward (Fig. 6*d*), and disappeared after 45 min (Fig. 6*e*). pSTAT5 was observed in the nucleus from the second minute. It accumulated there (Fig. 6, *b–e*), reached 50% of its maximum after 5–10 min, reached the maximum after 15–30 min, and decreased thereafter (Fig. 6*g*). STED microscopy showed that some pSTAT5 colocalized with microtubules; these pSTAT5 appeared as threads across the cytoplasm, as shown 5 min after the addition of IL-7 in the *enlarged image* in Fig. 6*c*.

Pretreating cells for 30 min with CytD + Col significantly altered the quantity of pSTAT5 in the cell, and 45 min after the IL-7 was added, most of the pSTAT5 was found in the inflated cytoplasm (Fig. 6*f*) instead of in the nucleus, as observed in the absence of inhibitors (Fig. 6*e*). Given that microtubules are clearly involved in the transport and translocation of pSTAT5 into the nucleus, we investigated the interaction between pSTAT5 and tubulin and two of the major molecular motor families that glide along microtubules: kinesins and dyneins (18). To do this, we activated CD4 T-cells with IL-7 (2 nM) for 1, 2, 3, 5, 10, 20, and 45 min and then harvested, washed, and lysed the cells in 0.5% Triton buffer. We immunoprecipitated protein complexes from centrifugation supernatants with anti-tubulin α, anti-UKHC (targeting the universal heavy chain common to all kinesin complexes), or anti-dynein intermediate chain and viewed Western blots after treatment with anti-pSTAT5 (Fig. 6*i*) or STAT5 (Fig. 6*j*). When the cytoplasmic membrane was lysed using ice-cold 0.5% Triton, pSTAT5 was immunoprecipitated with tubulin and UKHC in the first 5 min after IL-7 activation but was not detectable thereafter. When both the cytoplasmic and nuclear membranes were thoroughly lysed using 1% Triton buffer and cell freezing and thawing cycles, pSTAT5 and STAT5 were detectable for up to 20 and 45 min, respectively, after IL-7 activation when immunoprecipitated with tubulin (Fig. 6*k*). This observation suggests that the microtubules were carried away with the cell lysate centrifugation pellet under mild lysis conditions when microtubules anchor to the nucleus more than 2 min after IL-7 activation. Microtubules were released from nuclear membrane anchorage under stronger lysis conditions. This further suggests that microtubules grow from the membrane through the nucleus. The time shift observed in Fig. 6*k* between the pSTAT5 and STAT5 amounts immunoprecipitated with tubulin suggests that both phosphorylated and unphosphorylated STAT5 are carried along microtubules. Despite the presence of dynein in the cytoplasm (Fig. 6*j*, *lane C*), no STAT5 was coimmunoprecipitated with the dynein intermediate chain. These results seem to disqualify dynein from any involvement in pSTAT5 and STAT5 transport in CD4 T-cells and spotlight kinesins as molecular motor candidates for both the anterograde and retrograde transport of pSTAT5 and STAT5, respectively.

DISCUSSION

IL-7 induces a variety of responses in CD4 T-lymphocytes, primarily through the main common γc-signaling pathways JAK/STAT, Akt/PI3K, and MAPK (2). These pathways have been described as reaction cascades and are processed within

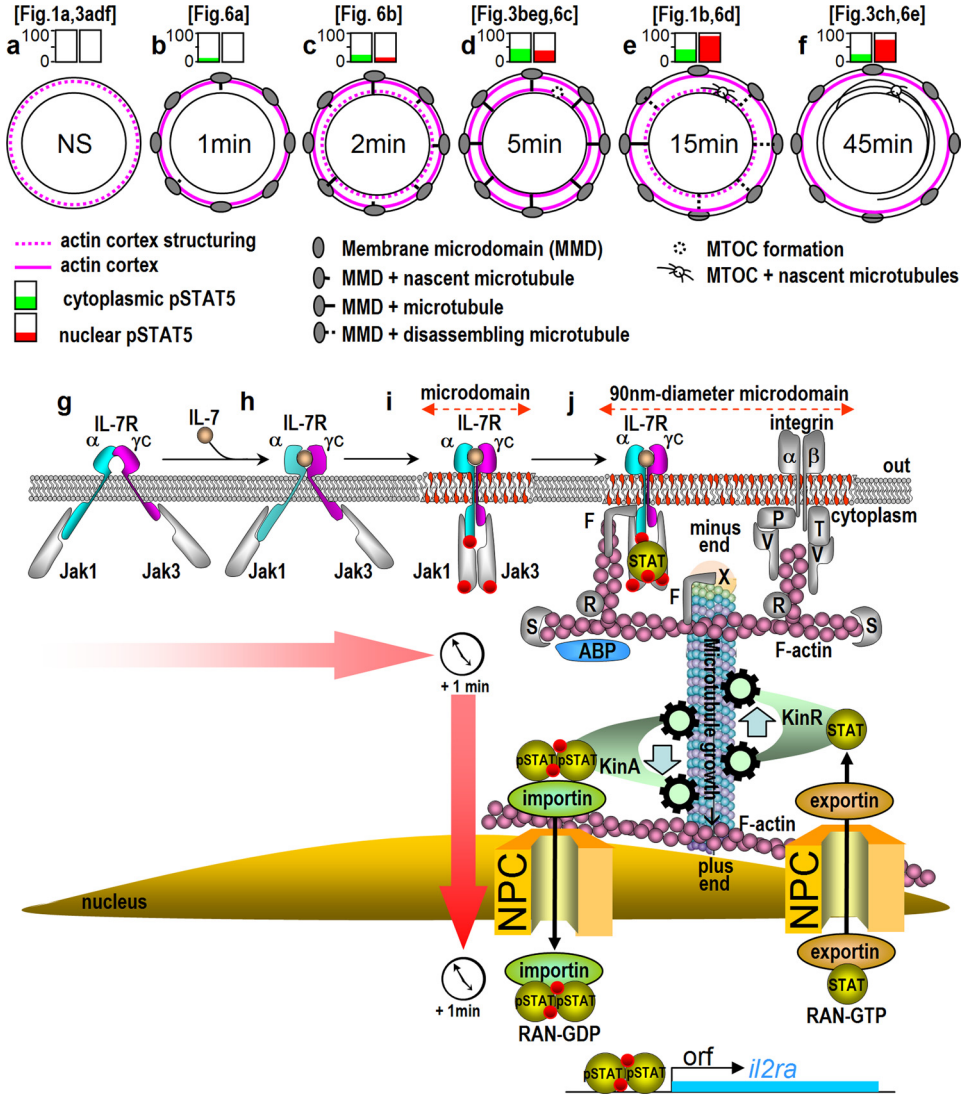

FIGURE 7. **Schematic of the IL-7-induced cytoskeleton organization and JAK/STAT signal transduction mechanism.** *a–f* sketch the formation of membrane microdomains and microtubules from 1 to 45 min after IL-7 activation of CD4 T-cells. *Black circles*, plasma and nuclear membranes of a single CD4+ T-cell; *top boxes*, percentages of cytoplasmic (*green*) and nuclear (*red*) pSTAT5; *bracketed indications* (*top*), correspondence with figures cited under "Results." *g*, IL-7-free IL-7Rα·γc heterodimers are embedded in the lipid bilayer, outside microdomains in quiescent cells. JAK1 and JAK3 are constitutively bound to IL-7Rα and IL-7Rγc, respectively. *h*, binding of IL-7 brings the transmembrane domains closer together. *i*, formation of the microdomains that hold the transmembrane domain straight and pull the cytoplasmic domains closer together. Phosphorylations are indicated by *red spheres* (*j*). The FERM proteins, moesin or ezrin (*F*), connect the submembrane FERM binding domain of IL-7Rα to F-actin. Integrin chains are linked to F-actin through praxillin (*P*) or talin (*T*) complexed to vinculin (*V*). *ABP*, actin-binding proteins; *S*, proteins inhibiting F-actin elongation; *R*, proteins involved in filament ramification. Microtubules are anchored to actin microfilament through the putative FERM protein candidate (*F*) and FERM binding protein (*X*) capping the microtubule minus-end. STAT5 is carried in retrograde kinesin cargo along microtubules toward the membrane (minus-end direction). STAT5 binds on IL-7Rα Tyr(P)-456 and then is phosphorylated by pJAK1·pJAK3. pSTAT5 is carried in the anterograde kinesin cargo as a dimer toward the nucleus (plus-end direction) and translocates through the nuclear pore (*NPC*) by means of the importin/Ran-GDP system. Minimum times for each mechanism step are indicated by *red arrows*.

the signaling complex, the signalosome, which is associated with the cytoplasmic domains of the IL-7 receptor rather than being free in the cytoplasm. This clustering of protein kinases with signaling intermediates optimizes substrate diffusion and presentation from one enzyme to another and organizes gradients of signaling intermediates (19). The molecular assembly of the reaction complexes that form the IL-7R signaling complex, or signalosome, needs to be further documented. Consistent with this, we have previously shown, by time-resolved microimaging and single molecule analyses, that IL-7 binds to its preassembled dimeric receptor then induces its compartmentalization in membrane microdomains and its interaction with the cytoskeleton meshwork (10). We have also demonstrated, by a proteomics approach, that IL-7R activation initiates the formation of signaling complexes involving signaling pathway proteins but also many components of the cytoskeleton and a number of proteins associated with membrane microdomains (10).

In the present study, we demonstrate, in human primary CD4 T-lymphocytes, that microdomains and cytoskeleton play important functional roles in structuring the IL-7R signaling complex and in regulating its signal transduction kinetics and intensity along the JAK/STAT pathway. Fig. 7, *a–f*, gives an outline of our observations in the form of a time-sequence representation of the membrane microdomain formation and cytoskeleton structuring induced by IL-7. In Fig. 7, *g–j*, we

interpret, in light of our results, the molecular mechanism of IL-7R-mediated JAK/STAT signal transduction, from IL-7 binding at the surface of CD4 T-cells to pSTAT5 transport into their nucleus.

We have previously shown that IL-7Rα·γc complexes assemble spontaneously by means of their ectodomains (11), as also demonstrated for homologous IL-2Rβ·γc complexes (20–22). IL-7Rα·γc diffuses rapidly in two dimensions at the surface of quiescent CD4 T-cells (10) (Fig. 7*g*). Very few membrane microdomains, labeled with CtxB targeting their GM1, were observed at the surface of these unactivated cells. Actin is mostly concentrated beneath the plasma membrane, and tubulin is very diffuse throughout the cytoplasm, not forming any highly structured patterns (Figs. 3 (*a*, *d*, and *f*) and 7*a*). When IL-7 is added and binds to its receptor, the IL-7Rα·γc ectodomains change shape, pull the long transmembrane domains closer together, and then bring their endodomains into close proximity, as proposed by Walsh and colleagues (6, 23) and summarized in Fig. 7, *g–i*. This mechanism has also been proposed for the IL-2Rβ·γc homologous system (22, 24). We found that a few min after IL-7 was added, about 300 membrane microdomains were formed over the entire surface of the T-cell (Figs. 1*b* and 6*a*). These were 90 nm in diameter (*i.e.* 50% larger than the practical resolution of our STED microscope). No such microdomains were observed after rapid treatment with cholesterol oxidase and sphingomyelinase, suggesting the enrichment in cholesterol and sphingomyelin in these structures. The fact that no such microdomains were present prior to the addition of IL-7 proves that they were not induced by the pentameric cholera toxin B used to label them. When IL-7 binding pulled IL-7Rα and γc endodomains together, JAK1 and JAK3 were tethered in close contact, and the JAK1·JAK3 complex recovered its tyrosine kinase activity and phosphorylated JAK1 (Tyr(P)-1034/Tyr(P)-1035) and JAK3 (Tyr(P)-980/Tyr(P)-981) themselves and IL-7Rα carboxyl-terminal Tyr (Tyr(P)-456) (Fig. 7*i*). Raft inhibitors delayed and reduced the phosphorylation of JAK1, JAK3, and STATs without abrogating it completely. Microdomain thickness and viscosity might regulate JAK1 and JAK3 phosphorylation through tilt control of the single transmembrane helical domain of the two chains, tethering their cytoplasmic domain and cognate kinase in close contact (10). Because STATs are phosphorylated by activated JAKs, inhibition of STAT phosphorylation should be a consequence of JAK inhibition.

It has been suggested that the IL-7Rα cytoplasmic sequence contains a FERM domain binding motif following the transmembrane domain (10). Another shorter FERM binding site might be questioned in the sequence of the γc cytoplasmic domain. Given that FERM proteins moesin and ezrin have been immunoprecipitated with activated IL-7-receptor complex (10), they might anchor rafted IL-7-activated receptor to F-actin and initiate the microfilament organization that structures the actin cortex lining the plasma membrane (25). This anchoring prevents IL-7R diffusion and stabilizes the recruitment of other receptors, such as integrin (10, 26). Tubulin anchors to actin microfilaments, potentially through ezrin at its minus-end (27), and polymerizes to form a microtubule that grows by its plus-end (28, 29), crosses the cytoplasm, and reaches the nucleus less than 2 min after the addition of IL-7 (Figs. 3*g* and 7*c*). Actin molecules assemble along the nucleus envelope to form microfilaments that form a tight cortex anchoring microtubule plus-ends. We found kinesin heavy chains, but not dynein, among the proteins coimmunoprecipitated with STAT5 from IL-7-activated cells. We also found STAT5 and pSTAT5 coimmunoprecipitated with kinesin heavy chains from IL-7-activated T-cells. This suggests that these microtubules may drive STAT5 with retrograde kinesin cargo toward the rafted IL-7R. STAT5 then binds to Tyr(P)-456 at the IL-7Rα carboxyl terminus and is phosphorylated on its Tyr-694 by pJAK1·pJAK3 (Fig. 7*j*). pSTAT5 dissociates from the receptors, dimerizes through Tyr(P)-694/Src homology 2 domain intermolecular association, and is driven by anterograde kinesins toward the nuclear pore. A nuclear localization signal has been found in STAT5 sequences (30); pSTAT5 might be imported through the nucleopore by the $\alpha\beta$-importin system (31). pSTAT5 dimers contribute, along with other factors, to the transcription of several genes, such as that coding for IL-2Rα. Unbound pSTAT5 dimers are then dephosphorylated. A nuclear export signal was also identified in the STAT5 sequences (32). STAT5 might be translocated out of the nucleus by the exportin system. It is then uploaded by retrograde kinesin and driven up to rafted receptors. In our studies, pSTAT5 translocation into the nucleus was fastest 5 min after the addition of IL-7 (Figs. 6*g* and 7*d*). It accumulated in the nucleus until the radial microtubules began to depolymerize 10–15 min after the addition of IL-7 and then gradually disappeared from the cytoplasm (15–30 min). Tubulin was then recruited by transversally growing microtubules from the MTOC 10 min after the addition of IL-7 (Figs. 3 (*c* and *h*) and 7*e*); our observations by pulsed STED microscopy did not show any colocalization of pSTAT5 with transversal microtubules from the MTOC system organized in a star pattern around the nucleus. Cellular pSTAT5, as assayed by cytometry, peaked 15 min after the addition of IL-7, corresponding to the total amount in the cytoplasm and nucleus. Microscopy showed that nuclear concentrations peaked 30 min after the addition of IL-7, whereas cytoplasmic pSTAT5 decreased from 10 min after the IL-7 addition (Fig. 6*g*).

Membrane microdomains have also been implicated in the T-cell receptor signaling cascade, where they are recruited transiently following receptor engagement to initiate the assembly of signaling machinery (33). Protein association with membrane microdomains is likely to be facilitated by raft coalescence following T-cell receptor triggering, a process promoted by cortical actin reorganization and enhanced by the engagement of costimulatory receptors, such as CD28, clustered at the immunological synapse (34). No such clustering is observed during the formation of IL-7R signaling complexes that are dispatched throughout the cell. Induction of cytoskeleton structuring has been described with many cytokines and chemokines but mostly over longer time spans. Pioneering studies on prolactin receptor (35), growth hormone receptor (36), and epidermal growth factor receptor (37) have suggested that machineries carried by the cytoskeleton might be involved in STAT5 and pSTAT5 distribution and proposed that rapid organization was involved. Here, in our study, we used super-

resolution optical microscopy to describe in detail how radial microtubules are formed within a few min of IL-7 activation, bridging plasma and nuclear membranes across the narrow cytoplasm of CD4 T-lymphocytes. This is the first time that this transient organization of radial microtubules, resembling the spokes of a wheel in an equatorial slice of the T-cell, has been described (Fig. 7*d*). We counted about one microtubule per membrane microdomain embedding IL-7R signaling complex. These microtubules bud from the actin cortex 1 min after the addition of IL-7 and then reach the nucleus in less than 1 min. They have a life span of 5–15 min. Kinesin-assisted transport along 1-μm-long microtubules has been described in the second range, but what role do these radial microtubules play in a cytoplasm that is so narrow that pSTAT5 should be able to cross it by passive diffusion in less than 1 s? When we added cytoskeleton inhibitors, the nuclear translocation of pSTAT5 was very slow, and it accumulated in the cytoplasm. In untreated IL-7-activated cells, pSTAT5 was found not only along microtubules, but microtubules might facilitate "fast track" nuclear import through a microtubule-importin interaction (38); the nuclear translocation of pSTAT5 might be the bottleneck in the JAK/STAT signal transduction induced by IL-7 and may require active molecular motor assistance for guidance and ushering, not for speed.

In more general terms, our functional approach has led to the discovery of IL-7 signal transduction mechanisms involving membrane microdomains and transient cytoskeleton structuring that regulate the kinetics and amplification of the JAK/STAT pathway that is central to CD4 T-cell responses. Membrane microdomains optimize the receptor response, and microtubules and molecular motors shorten signal transduction time from membrane to nucleus pore and secure the nuclear translocation of transcription factors, rapidly priming the cell response. This is consistent with the sensing role of CD4 T-cells that is so central to the immune survey and response.

Acknowledgments—We thank Dr. Andres Alcover and Dr. Rémi Lasserre (Institut Pasteur) for helpful discussions. We thank Pascal Roux and Emmanuelle Perret (Plate-Forme d'Imagerie Dynamique, Institut Pasteur) for expertise and technical help in microscopy and Mark Jones (Transcriptum) for text editing. We extend our gratitude to the volunteer blood donors and staff at the Etablissement Français du Sang (Centre Necker-Cabanel-Paris).

REFERENCES

1. Mackall, C. L., Fry, T. J., and Gress, R. E. (2011) Harnessing the biology of IL-7 for therapeutic application. *Nat. Rev. Immunol.* **11,** 330–342
2. Rochman, Y., Spolski, R., and Leonard, W. J. (2009) New insights into the regulation of T cells by γ_c family cytokines. *Nat. Rev. Immunol.* **9,** 480–490
3. Goodwin, R. G., Lupton, S., Schmierer, A., Hjerrild, K. J., Jerzy, R., Clevenger, W., Gillis, S., Cosman, D., and Namen, A. E. (1989) Human interleukin 7. Molecular cloning and growth factor activity on human and murine B-lineage cells. *Proc. Natl. Acad. Sci. U.S.A.* **86,** 302–306
4. Goodwin, R. G., Friend, D., Ziegler, S. F., Jerzy, R., Falk, B. A., Gimpel, S., Cosman, D., Dower, S. K., March, C. J., and Namen, A. E. (1990) Cloning of the human and murine interleukin-7 receptors. Demonstration of a soluble form and homology to a new receptor superfamily. *Cell* **60,** 941–951
5. Park, L. S., Martin, U., Garka, K., Gliniak, B., Di Santo, J. P., Muller, W., Largaespada, D. A., Copeland, N. G., Jenkins, N. A., Farr, A. G., Ziegler, S. F., Morrissey, P. J., Paxton, R., and Sims, J. E. (2000) Cloning of the murine thymic stromal lymphopoietin (TSLP) receptor. Formation of a functional heteromeric complex requires interleukin 7 receptor. *J. Exp. Med.* **192,** 659–670
6. Walsh, S. T. (2012) Structural insights into the common γ-chain family of cytokines and receptors from the interleukin-7 pathway. *Immunol. Rev.* **250,** 303–316
7. Alves, N. L., van Leeuwen, E. M., Derks, I. A., and van Lier, R. A. (2008) Differential regulation of human IL-7 receptor α expression by IL-7 and TCR signaling. *J. Immunol.* **180,** 5201–5210
8. Colle, J. H., Moreau, J. L., Fontanet, A., Lambotte, O., Delfraissy, J. F., and Thèze, J. (2007) The correlation between levels of IL-7Rα expression and responsiveness to IL-7 is lost in CD4 lymphocytes from HIV-infected patients. *AIDS* **21,** 101–103
9. Park, J. H., Yu, Q., Erman, B., Appelbaum, J. S., Montoya-Durango, D., Grimes, H. L., and Singer, A. (2004) Suppression of IL7Rα transcription by IL-7 and other prosurvival cytokines. A novel mechanism for maximizing IL-7-dependent T cell survival. *Immunity* **21,** 289–302
10. Rose, T., Pillet, A. H., Lavergne, V., Tamarit, B., Lenormand, P., Rousselle, J. C., Namane, A., and Thèze, J. (2010) Interleukin-7 compartmentalizes its receptor signaling complex to initiate CD4 T lymphocyte response. *J. Biol. Chem.* **285,** 14898–14908
11. Rose, T., Lambotte, O., Pallier, C., Delfraissy, J. F., and Colle, J. H. (2009) Identification and biochemical characterization of human plasma soluble IL-7R. Lower concentrations in HIV-1-infected patients. *J. Immunol.* **182,** 7389–7397
12. Leonard, W. J., Imada, K., Nakajima, H., Puel, A., Soldaini, E., and John, S. (1999) Signaling via the IL-2 and IL-7 receptors from the membrane to the nucleus. *Cold Spring Harb. Symp. Quant. Biol.* **64,** 417–424
13. Hell, S. W., and Wichmann, J. (1994) Breaking the diffraction resolution limit by stimulated emission. Stimulated-emission-depletion fluorescence microscopy. *Opt. Lett.* **19,** 780–782
14. Willig, K. I., Harke, B., Medda, R., and Hell, S. W. (2007) STED microscopy with continuous wave beams. *Nat. Methods* **4,** 915–918
15. Eggeling, C., Ringemann, C., Medda, R., Schwarzmann, G., Sandhoff, K., Polyakova, S., Belov, V. N., Hein, B., von Middendorff, C., Schönle, A., and Hell, S. W. (2009) Direct observation of the nanoscale dynamics of membrane lipids in a living cell. *Nature* **457,** 1159–1162
16. He, H. T., and Marguet, D. (2011) Detecting nanodomains in living cell membrane by fluorescence correlation microscopy. *Annu. Rev. Phys. Chem.* **62,** 417–436
17. Lenne, P. F., Wawrezinieck, L., Conchonaud, F., Wurtz, O., Boned, A., Guo, X. J., Rigneault, H., He, H. T., and Marguet, D. (2006) Dynamic molecular confinement in the plasma membrane by microdomains and the cytoskeleton meshwork. *EMBO J.* **25,** 3245–3256
18. Schliwa, M., and Woehlke, G. (2003) Molecular motors. *Nature* **422,** 759–765
19. Grecco, H. E., Schmick, M., and Bastiaens, P. I. (2011) Signaling from the living plasma membrane. *Cell* **144,** 897–909
20. Pillet, A., Bugault, F., Thèze, J., Chakrabarti, L., and Rose, T. (2009) A programmed switch from IL-15- to IL-2-dependent activation in human NK cells. *J. Immunol.* **182,** 6267–6277
21. Pillet, A. H., Juffroy, O., Mazard-Pasquier, V., Moreau, J. L., Gesbert, F., Chastagner, P., Colle, J. H., Thèze, J., and Rose, T. (2008) Human IL-Rβ chains form IL-2 binding homodimers. *Eur. Cytokine Netw.* **19,** 49–59
22. Pillet, A. H., Lavergne, V., Gesbert, F., Mazard-Pasquier, V., Thèze, J., and Rose, T. (2010) IL-2 induces conformational changes in its preassembled receptor core which then migrates in lipid raft and binds to cytoskeleton meshwork. *J. Mol. Biol.* **403,** 671–692
23. McElroy, C. A., Holland, P. J., Zhao, P., Lim, J. M., Wells, L., Eisenstein, E., and Walsh, S. T. (2012) Structural reorganization of the interleukin-7 signaling complex. *Proc. Natl. Acad. Sci. U.S.A.* **109,** 2503–2508
24. Wang, X., Rickert, M., and Garcia, K. C. (2005) Structure of the quaternary complex of interleukin-2 with its α, β, and γc receptors. *Science* **310,** 1159–1163
25. Viola, A., and Gupta, N. (2007) Tether and trap. Regulation of membrane-raft dynamics by actin-binding proteins. *Nat. Rev. Immunol.* **7,** 889–896
26. Kitazawa, H., Muegge, K., Badolato, R., Wang, J. M., Fogler, W. E., Ferris,

D. K., Lee, C. K., Candéias, S., Smith, M. R., Oppenheim, J. J., and Durum, S. K. (1997) IL-7 activates $\alpha 4\beta 1$ integrin in murine thymocytes. *J. Immunol.* **159,** 2259–2264
27. Lasserre, R., Charrin, S., Cuche, C., Danckaert, A., Thoulouze, M. I., de Chaumont, F., Duong, T., Perrault, N., Varin-Blank, N., Olivo-Marin, J. C., Etienne-Manneville, S., Arpin, M., Di Bartolo, V., and Alcover, A. (2010) Ezrin tunes T-cell activation by controlling Dlg1 and microtubule positioning at the immunological synapse. *EMBO J.* **29,** 2301–2314
28. Akhmanova, A., and Steinmetz, M. O. (2008) Tracking the ends: a dynamic protein network controls the fate of microtubule tips. *Nat. Rev. Mol. Cell Biol.* **9,** 309–322
29. Jiang, K., and Akhmanova, A. (2011) Microtubule tip-interacting proteins. A view from both ends. *Curr. Opin. Cell Biol.* **23,** 94–101
30. Melen, K., Kinnunen, L., and Julkunen, I. (2001) Arginine/lysine-rich structural element is involved in interferon-induced nuclear import of STATs. *J. Biol. Chem.* **276,** 16447–16455
31. Fagerlund, R., Mélen, K., Kinnunen, L., and Julkunen, I. (2002) Arginine/lysine-rich nuclear localization signals mediate interactions between dimeric STATs and importin $\alpha 5$. *J. Biol. Chem.* **277,** 30072–30078
32. Mattaj, I. W., and Englmeier, L. (1998) Nucleocytoplasmic transport. The soluble phase. *Annu. Rev. Biochem.* **67,** 265–306
33. Chichili, G. R., and Rodgers, W. (2009) Cytoskeleton-membrane interactions in membrane raft structure. *Cell Mol. Life Sci.* **66,** 2319–2328
34. Lasserre, R., and Alcover, A. (2010) Cytoskeletal cross-talk in the control of T cell antigen receptor signaling. *FEBS Lett.* **584,** 4845–4850
35. Zoubiane, G. S., Valentijn, A., Lowe, E. T., Akhtar, N., Bagley, S., Gilmore, A. P., and Streuli, C. H. (2004) A role for the cytoskeleton in prolactin-dependent mammary epithelial cell differentiation. *J. Cell Sci.* **117,** 271–280
36. Phung-Koskas, T., Pilon, A., Poüs, C., Betzina, C., Sturm, M., Bourguet-Kondracki, M. L., Durand, G., and Drechou, A. (2005) STAT5B-mediated growth hormone signaling is organized by highly dynamic microtubules in hepatic cells. *J. Biol. Chem.* **280,** 1123–1131
37. Lopez-Perez, M., and Salazar, E. P. (2006) A role for the cytoskeleton in STAT5 activation in MCF7 human breast cancer cells stimulated with EGF. *Int. J. Biochem. Cell Biol.* **38,** 1716–1728
38. Cangiani, A., and Natalini, R. (2010) A spatial model of cellular molecular trafficking including active transport along microtubules. *J. Theor. Biol.* **267,** 614–625